Soft-Switching Bidirectional Isolated Full-Bridge Converter With Active and Passive Snubbers

Tsai-Fu Wu, *Senior Member, IEEE*, Jeng-Gung Yang, Chia-Ling Kuo, and Yung-Chun Wu

***Abstract*—A bidirectional isolated full-bridge dc–dc converter with a conversion ratio around nine times, soft start-up, and soft-switching features for battery charging/discharging is proposed in this paper. The converter is equipped with an active flyback and two passive capacitor–diode snubbers, which can reduce voltage and current spikes and reduce voltage and current stresses, while it can achieve near zero-voltage-switching and zero-current-switching soft-switching features. In this paper, the operational principle of the proposed converter is first described, and its analysis and design are then presented. A 1.5-kW prototype with a low-side voltage of 48 V and a high-side voltage of 360 V has been implemented, from which measured results have verified the discussed features.**

***Index Terms*—Bidirectional, snubbers, soft switching.**

I. Introduction

In renewable dc supply systems, batteries are usually required to back up power for electronic equipment. The voltage levels of the batteries are typically much lower than the dc-bus voltage. Bidirectional converters for charging/discharging the batteries are therefore required. In past studies, bridge-type bidirectional isolated converters have been widely applied to fuel cell and electric vehicle driving systems [1]–[6]. For raising power level, a dual full-bridge configuration is usually adopted [7]–[18], and their low and high sides are typically configured with boost- and buck-type topologies, respectively. However, component stress, switching loss, and electromagnetic interference (EMI) noise are increased due to diode-reverse-recovery current and MOSFET drain–source voltage, resulting in low reliability. A more severe issue is due to leakage inductance of the isolation transformer, which will result in high-voltage spike during switching transition. A possible solution is to pre-excite the leakage inductance to raise its current level up to that of the current-fed inductor, which can reduce their current difference and, in turn, reduce voltage spike. However, since the current level varies with load condition, it is hard to tune the switching timing to match these two currents. Thus, a passive or an active snubber circuit is still needed.

Manuscript received February 3, 2012; revised March 28, 2012; accepted April 29, 2012. Date of publication May 13, 2013; date of current version August 23, 2013.

T.-F. Wu is with the Elegant Power Electronic Application Research Laboratory, Department of Electrical Engineering, National Tsing Hua University, Hsinchu 300, Taiwan (e-mail: tfwu@ee.nthu.edu.tw).

J.-G. Yang and C.-L. Kuo are with the Elegant Power Application Research Center, Department of Electrical Engineering, National Chung Cheng University, Minxiong 621, Taiwan (e-mail: d00415002@ccu.edu.tw).

Y.-C. Wu is with the Innovative Design and Energy Application Laboratory, Department of Aeronautical Engineering, National Formosa University, Huwei 632, Taiwan (e-mail: ycwu@nfu.edu.tw).

Color versions of one or more of the figures in this paper are available online at http://ieeexplore.ieee.org.

Digital Object Identifier 10.1109/TIE.2013.2262746

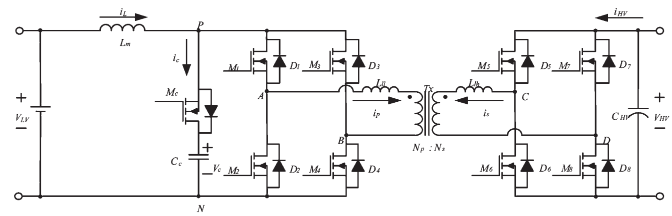

Fig. 1. Bidirectional isolated full-bridge dc–dc converter with an active clamp snubber.

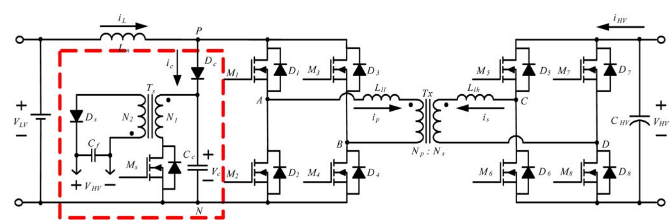

Fig. 2. Bidirectional isolated full-bridge dc–dc converter with a flyback snubber (type A).

Passive and active clamp circuits were proposed to suppress the voltage spike due to the current difference between the current-fed inductor and leakage inductance currents [13], [14]. A conventional passive approach is employing a resistor–capacitor–diode snubber to clamp the voltage, and the energy absorbed in the buffer capacitor is dissipated on the resistor, resulting in low efficiency. On the other hand, a simple active clamping circuit [13] was proposed, which is shown in Fig. 1. However, the resonant current will flow through the main switches, increasing current stress significantly. An isolated bidirectional converter with a flyback snubber was therefore proposed [18], [19], which is shown in Fig. 2. The flyback snubber can recycle the absorbed energy which is stored in the clamping capacitor C_C, while without current flowing through the main switches. It can also clamp the voltage to a desired value just slightly higher than the voltage across the low-side transformer. Since the snubber current does not circulate through the main switches, current stress can be reduced a lot under heavy-load condition. Furthermore, the flyback snubber can be controlled to precharge the high-side capacitor to avoid in-rush current during a start-up period. However, the low- and high-side switches are operated with hard switching turnoff, resulting in high-voltage spikes.

To solve the aforementioned problem, we first introduce two buffer capacitors (C_{b1} and C_{b2}) connected in parallel with the upper legs of the voltage-fed bridge, as shown in Fig. 3. With

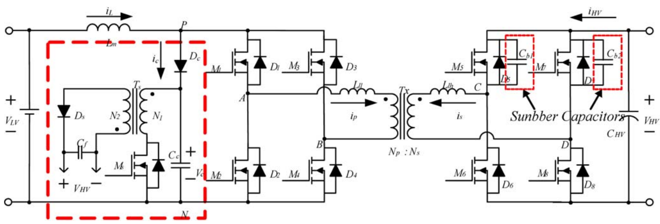

Fig. 3. Bidirectional isolated full-bridge dc–dc converter with a flyback snubber and paralleled snubber capacitors C_{b1} and C_{b2} (type B).

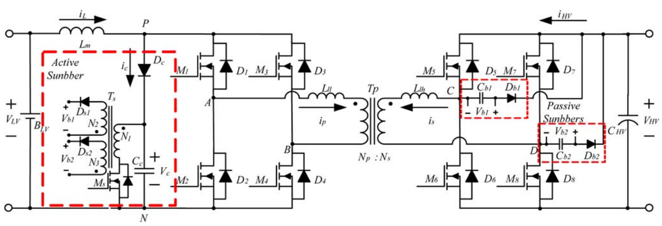

Fig. 4. Proposed soft-switching bidirectional isolated full-bridge converter with an active flyback and two passive capacitor–diode snubbers (type C).

these two buffer capacitors, the low- and high-side switches can operate with near zero-voltage switching (ZVS) and zero-current switching (ZCS). However, when it is operated in step-down conversion, these capacitors will resonate with leakage inductance of the transformer, causing EMI noise and increasing switching loss. Thus, two passive capacitor–diode snubbers are proposed to supplement the active flyback snubber, as shown in Fig. 4. The proposed snubber configuration cannot only reduce the voltage spike caused by the current difference between the leakage inductance and current-fed inductor currents but also can relieve the drawbacks of high-current and high-voltage stresses imposed on the main switches at both turn-on and turnoff transitions. Moreover, it can achieve near ZVS and ZCS for the switches on both sides of the transformer.

II. Configuration and Operation

The proposed soft-switching bidirectional isolated full-bridge converter with an active flyback and two passive capacitor–diode snubbers is shown in Fig. 4. It can be operated with two types of conversions: step-up conversion and step-down conversion. Fig. 4 consists of a current-fed switch bridge, an active flyback snubber at the low-voltage side, a voltage-fed switch bridge, and a passive snubber pair at the high-voltage side. Inductor L_m performs output filtering when power flows from the high-voltage side to the low-voltage side, which is denoted as a step-down conversion. On the other hand, it works in the step-up conversion. Moreover, snubber capacitor C_C and diode D_C are used to absorb the current difference between current-fed inductor current i_L and leakage inductance current i_P of isolation transformer T_P during switching commutation. The flyback snubber is operated to transfer the energy stored in snubber capacitor C_C to buffer capacitors C_{b1} and C_{b2}, and voltage V_C can drop to zero. Thus, the voltage stresses of switches $M_1 \sim M_4$ can be limited to a lower level, achieving near ZCS turnoff. The main merits of the proposed snubber include no spike current circulating through the switches and achieving soft-switching features. Note that high spike current can result in charge migration, over current density, and extra magnetic force which will deteriorate in MOSFET carrier density, channel width, and wire bonding and, in turn, increase its conduction resistance.

In the step-up conversion, switches $M_1 \sim M_4$ are controlled, and the body diodes of switches $M_5 \sim M_8$ serve as a rectifier. In the step-down conversion, switches $M_5 \sim M_8$ are controlled, and the body diodes of switches $M_1 \sim M_4$ operate as a full-bridge rectifier. To simplify the steady-state analysis, several assumptions are made as follows.

1) All components are ideal except that the transformer is associated with leakage inductance.
2) Inductor L_m is large enough to keep the current i_L constant over a switching period.
3) Snubber capacitor C_C is much larger than the parasitic capacitance of switches $M_1 \sim M_8$.

A. Step-Up Conversion

In the step-up conversion, switches $M_1 \sim M_4$ are operated like a boost converter, where switch pairs (M_1, M_2) and (M_3, M_4) conduct to store energy in L_m. At the high-voltage side, body diodes $D_5 \sim D_8$ of switches $M_5 \sim M_8$ will conduct to transfer power to C_{HV}. When switch pairs (M_1, M_2) and (M_3, M_4) are switched to (M_1, M_4) or (M_2, M_3), current difference i_C $(= i_L - i_P)$ will charge capacitor C_C until i_P rises up to i_L, and capacitor voltage V_C will be clamped to $V_{\mathrm{HV}} \cdot (N_P/N_S)$, achieving near ZCS turnoff for M_2 or M_4. In the meantime, high-side current i_S has the priority flowing through one of the two passive capacitor–diode snubbers, and either C_{b1} or C_{b2} will be fully discharged before diode D_5 or D_7 conducts. When switch pair (M_1, M_4) or (M_2, M_3) is switched back to (M_1, M_2) and (M_3, M_4), switch M_2 or M_4 can have near ZCS turn-on feature due to leakage inductance L_{ll} limiting the di/dt of high-side diode-reverse-recovery current. The flyback snubber operates simultaneously to discharge snubber capacitor C_C and transfer the stored energy to buffer capacitors C_{b1} and C_{b2}. With the flyback snubber, the energy absorbed in C_C will not flow through switches $M_1 \sim M_4$, which can reduce their current stresses dramatically when the leakage inductance of the isolation transformer is significant.

The key voltage and current waveforms of the converter operated in the step-up conversion are shown in Fig. 5. A detailed description of the converter operation over a half-switching cycle is presented as follows.

1) **Mode 1** $[t_0 \leq t < t_1]$: Before t_0, all of the four switches $M_1 \sim M_4$ are turned on. Inductor L_m is charged by V_{LV}. At t_0, M_1 and M_4 remain conducting, while M_2 and M_3 are turned off. Then, clamping diode D_C conducts, and snubber capacitor C_C is charged by the current difference i_C. In this mode, the flyback snubber still stays in the OFF state. The equivalent circuit is shown in Fig. 6(a).
2) **Mode 2** $[t_1 \leq t < t_2]$: In this mode, leakage inductance current i_P will start to track current i_L, and buffer capacitor C_{b1} will start to release energy. At time t_2, current i_P is equal to current i_L, the voltage of switches M_2 and M_3 and capacitor C_C will reach the maximum value simultaneously, and its equivalent circuit is shown in

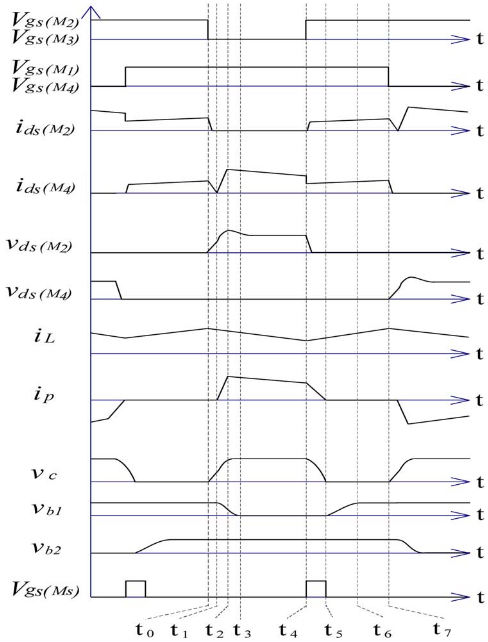

Fig. 5. Key voltage and current waveforms of the proposed converter operated in the step-up conversion.

Fig. 6(b). A near ZCS soft switching is therefore attained during t_0 to t_2.

3) **Mode 3** $[t_2 \leq t < t_3]$: Before t_3, the energy stored in buffer capacitor C_{b1} is not fully discharged yet. Thus, the capacitor will not stop discharging until V_{b1} drops to zero. The equivalent circuit is shown in Fig. 6(c).

4) **Mode 4** $[t_3 \leq t < t_4]$: When the energy stored in C_{b1} has been completely released to the output at t_3, diode D_5 will conduct. The circuit operation over this time interval is identical to a regular turnoff state of a conventional current-fed full-bridge converter. The equivalent circuit is shown in Fig. 6(d).

5) **Mode 5** $[t_4 \leq t < t_5]$: At t_4, all of the four switches $M_1 \sim M_4$ are turned on again, and switch M_S of the flyback snubber is turned on synchronously. Switches M_2 and M_3 achieve a ZCS turn-on soft-switching feature due to L_{ll}, and current i_P drops to zero gradually. In the flyback snubber, the energy stored in capacitor C_C will be delivered to the magnetizing inductance of transformer T_S. The equivalent circuit is shown in Fig. 6(e).

6) **Mode 6** $[t_5 \leq t < t_6]$: When switch M_S is turned off at t_5, capacitor voltage V_C drops to zero, and the energy stored in the magnetizing inductance will be transferred to buffer capacitor C_{b1}. In this mode, the time interval of driving signal $V_{gs(Ms)}$ is slightly longer than the discharging time of capacitor C_C. The purpose is to ensure that the energy stored in capacitor C_C can be completely released, creating a ZCS operational opportunity for switch M_2 or M_4 at the next turnoff transition. The equivalent circuit is shown in Fig. 6(f).

7) **Mode 7** $[t_6 \leq t < t_7]$: At t_6, the energy stored in the magnetizing inductance of transformer T_S was completely transferred to buffer capacitor C_{b1}, and the circuit operation is identical to a regular turn-on state of a conventional current-fed converter. Its equivalent circuit is shown in Fig. 6(g). The circuit operation stops at t_7 and completes a half-switching cycle.

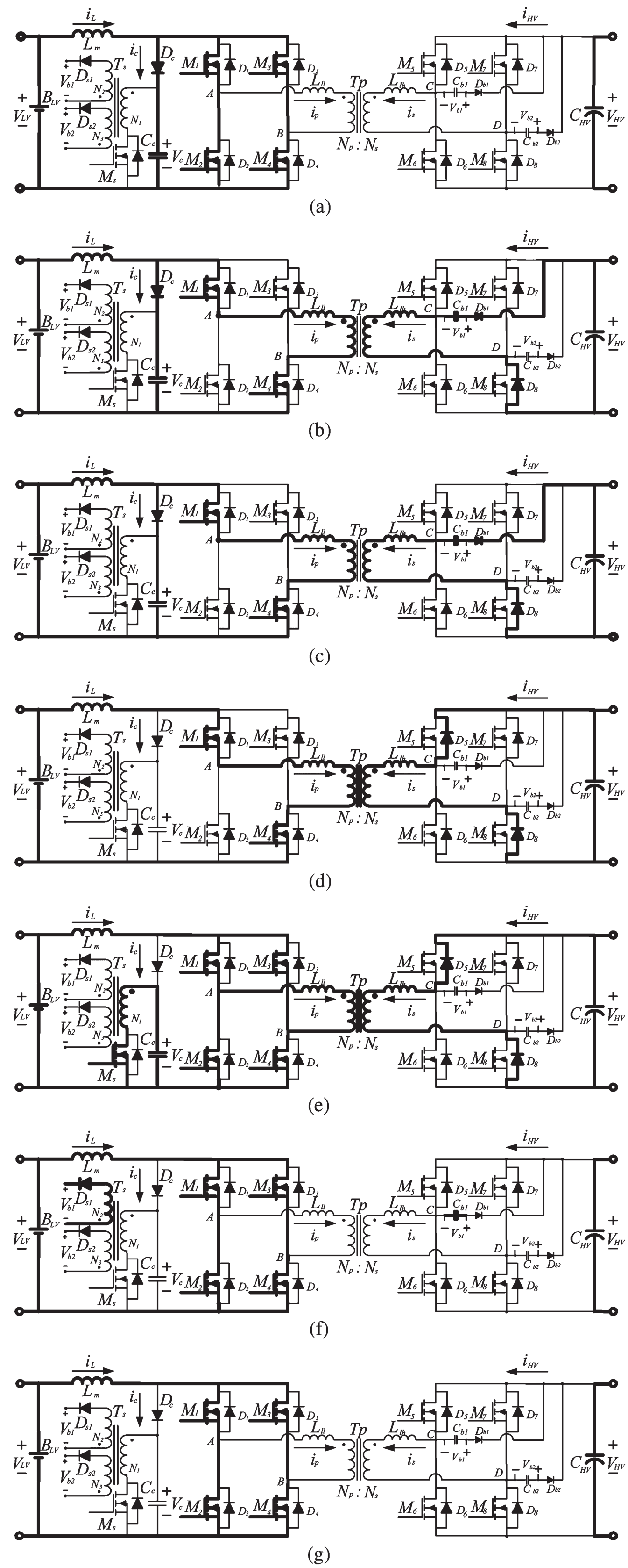

Fig. 6. Operation modes of the step-up conversion. (a) Mode 1. (b) Mode 2. (c) Mode 3. (d) Mode 4. (e) Mode 5. (f) Mode 6. (g) Mode 7.

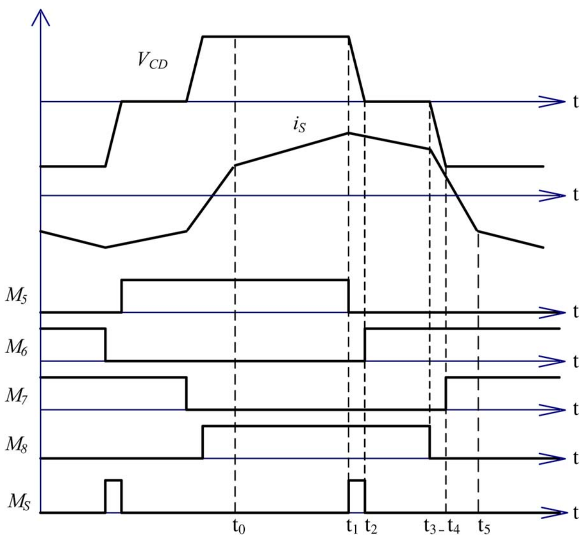

Fig. 7. Key voltage and current waveforms of the proposed converter operated in the step-down conversion.

B. Step-Down Conversion

In the analysis, the leakage inductance of the transformer at the low-voltage side is reflected to the high-voltage side, in which equivalent inductance L^*_{eq} equals $(L_{lh} + L_{ll} \cdot N_s^2/N_p^2)$.

In the step-down conversion, switches $M_5 \sim M_8$ are operated like a buck converter in which switch pairs (M_5, M_8) and (M_6, M_7) take turns conducting to transfer power from capacitor C_{HV} to battery B_{LV}. For alleviating leakage inductance effect on voltage spike, switches $M_5 \sim M_8$ are operated with phase-shift control, achieving ZVS turn-on features. Although there is no need to absorb the current difference between i_L and i_P, capacitor C_C can help clamp the voltage ringing due to L^*_{eq} and the parasitic capacitance of $M_1 \sim M_4$. With the two passive capacitor–diode snubbers, switches M_6 and M_8 can achieve near ZCS turnoff.

The key voltage and current waveforms of the converter operated in the step-down conversion are shown in Fig. 7. A detailed description of its operation over a half-switching cycle is presented as follows.

1) **Mode 1** $[t_0 \le t < t_1]$: In this mode, switches M_5 and M_8 are turned on, while M_6 and M_7 are in the OFF state. The high-side voltage V_{HV} is crossing the transformer, and it is, in fact, crossing the equivalent inductance L^*_{eq} and drives current i_S to rise with the slope of $V_{\text{HV}}/L^*_{\text{eq}}$. With the transformer current increasing toward the load-current level at t_1, the body diodes (D_1 and D_4) are conducting to transfer power, and the voltage across the transformer terminals on the low-voltage side changes immediately to reflect the voltage from the high-voltage side. The equivalent circuit is shown in Fig. 8(a).
2) **Mode 2** $[t_1 \le t < t_2]$: At t_1, switch M_8 remains conducting, while M_5 is turned off. The body diode of M_6 then starts conducting the freewheeling leakage current. The transformer current i_S reaches the load-current level at t_1, and V_{AB} rises to the reflected voltage $(V_{\text{HV}} \cdot N_P/N_S)$. Clamping diode D_C starts conducting the resonant current of L^*_{eq} and the parasitic capacitance of $M_1 \sim M_4$. At the same time, switch M_S of the flyback snubber is turned on and starts transferring the energy stored in capacitor C_C to buffer capacitors C_{b1} and C_{b2}. The process ends at t_2 when the resonance goes through a half resonant cycle and is blocked by clamping diode D_C. With the flyback snubber, the voltage of capacitor C_C will be clamped to a desired level just slightly higher than the voltage of $V_{ds(M4)}$. The equivalent circuit is shown in Fig. 8(b).

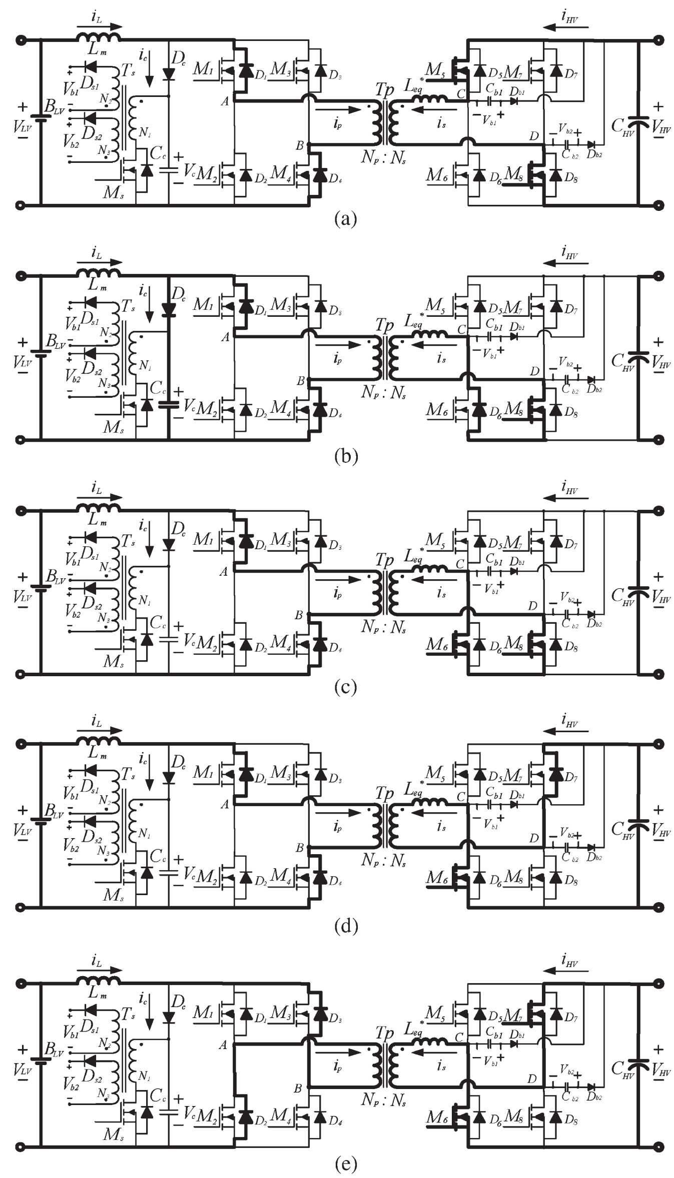

Fig. 8. Operation modes of the step-down conversion. (a) Mode 1. (b) Mode 2. (c) Mode 3. (d) Mode 4. (e) Mode 5.

3) **Mode 3** $[t_2 \le t < t_3]$: At t_2, the body diode of switch M_6 is conducting, and switch M_6 can be turned on with ZVS. The equivalent circuit is shown in Fig. 8(c).
4) **Mode 4** $[t_3 \le t < t_4]$: At t_3, switch M_6 remains conducting, while M_8 is turned off. Buffer capacitor C_{b2} is discharging by the freewheeling current. When C_{b2} is fully discharged, a near ZCS turnoff condition is therefore attained, and the body diode of M_7 then starts conducting the freewheeling current. The equivalent circuit is shown in Fig. 8(d).

5) **Mode 5** $[t_4 \leq t < t_5]$: At t_4, with the body diode of switch M_7 conducting, M_7 can be turned on with ZVS. Over this time interval, the active switches change to the other pair of switches, and the voltage across the transformer reverses its polarity. The circuit operation stops at t_5 and completes a half-switching cycle. The equivalent circuit is shown in Fig. 8(e).

III. Design and Practical Consideration of Snubbers

The purpose of using an active flyback snubber is to transfer energy from snubber capacitor C_C to buffer capacitors C_{b1} and C_{b2}, which can attain a near ZCS soft-switching feature. To reduce high-voltage spike occurring on switch M_S, the flyback snubber is operated in discontinuous conduction mode, and the key components of the proposed snubber are designed as follows.

A. Snubber Capacitor C_C

For clamping the switch voltage at the low-voltage side, snubber capacitor C_C needs to satisfy the following inequality:

$$C_C \geq \frac{L_{\text{eq}} \cdot (i_L \cdot i_p)^2}{V_C^2} \tag{1}$$

where $L_{\text{eq}} = L_{ll} + L_{lh}.N_p^2/N_s^2$.

B. Leakage Inductance

When the proposed converter is operated under step-down conversion, diode reverse recovery will cause high-current spike during switching transition. The leakage inductance of the transformer can not only limit diode-reverse-recovery current but also can achieve ZVS turn-on with a phase-shift operation manner. The leakage inductance needs to satisfy

$$i_S > \sqrt{\frac{2}{L_{\text{eqh}}}\left(\frac{4}{3}C_{\text{MOS}}V_{\text{in}}^2 + \frac{1}{2}C_{\text{TR}}V_{\text{in}}^2\right)} \tag{2}$$

where $L_{\text{eqh}} = L_{lh} + L_{ll} \cdot N_s^2/N_p^2$. However, large leakage inductance will cause high current difference during the step-up conversion, and the flyback snubber needs to process a high power level.

C. Flyback Snubber

During the interval of $[t_0, t_2]$, a high transient voltage occurs under the step-up conversion due to the current difference between the leakage inductance and current-fed inductor currents, which can be suppressed by D_C and C_C. The energy stored in capacitor C_C is transferred to buffer capacitors C_{b1} and C_{b2} by the flyback snubber. The power rating of the flyback snubber can be expressed as

$$P_{\text{FB}} = 0.5C_C \cdot V_C^2 \cdot f_S \tag{3}$$

where f_S is the switching frequency.

D. Magnetizing Inductance of Flyback Snubber

To ensure that snubber capacitor C_C can be fully discharged by the flyback snubber, the turn-on time of M_S (T_{ON}) cannot be longer than 1/4 resonant cycle of the magnetizing inductance and C_C. Thus, the magnetizing inductance of the flyback snubber should satisfy the following inequality:

$$L_{mf} > \frac{4T_{\text{ON}}^2}{\pi^2 C_C} \tag{4}$$

where T_{ON} is the conduction time of switches $M_1 \sim M_4$ in the step-up conversion.

E. Buffer Capacitors C_{b1} and C_{b2}

When the converter is operated in the step-down conversion, capacitors C_{b1} and C_{b2} can share current i_S, and $V_{ds(M6)}$ and $V_{ds(M8)}$ will rise up with a lower slope at switches M_6 and M_8 turnoff transition, reducing switching loss. If the power rating becomes higher, buffer capacitors C_{b1} and C_{b2} can be enlarged to achieve near ZCS turnoff. On the other hand, when the converter is operated in the step-up conversion, snubber capacitor C_C will be fully discharged by the proposed operation scheme. When switches $M_1 \sim M_4$ are switched to either (M_1, M_4) or (M_2, M_3) conducting, current difference i_C $(= i_L - i_P)$ will first charge capacitor C_C. Meanwhile, current i_P can start to rise up because of C_{b1} and C_{b2} holding voltage V_{HV}, which can reduce duty loss. For C_{b1} and C_{b2} being charged up to V_{HV} by the flyback snubber, they need to satisfy the following inequality:

$$C_{b1}, C_{b2} \leq \frac{C_C \cdot V_C^2}{V_{\text{HV}}^2}. \tag{5}$$

F. Snubber Diodes D_{b1} and D_{b2}

In the analysis, if capacitors C_{b1} and C_{b2} are connected in parallel with the upper legs of the voltage-fed bridge directly, they will resonate with the leakage inductance during switching transition in the step-down conversion, increasing switching loss. Thus, two snubber diodes D_{b1} and D_{b2} are introduced to connect with C_{b1} and C_{b2} in series, respectively, and the ringing current through the high-side switches can be blocked effectively.

G. Soft Start-Up

High inrush current is a start-up problem with the step-up conversion. The initial high-side voltage V_{HV} should not be lower than $V_{\text{LV}} \cdot N_S/N_P$ to avoid inrush current. When V_{HV} is not high enough, the controller will drive the flyback snubber to precharge high-side capacitor C_{HV} to achieve a soft start-up feature.

IV. Experimental Results

To verify the operational principle and performance of the proposed converter, three experimental prototypes of 1.5 kW, the converter shown in Fig. 2 (type A), the one shown in Fig. 3 (type B), and the proposed, shown in Fig. 4 (type C), were designed and built. The low-side voltage is 42–54 V, and the

TABLE I
SPECIFICATIONS OF PROTOTYPE

Low-side Voltage	48 V (nominal value)
High-side Voltage	360 V
Maximum Output Power	1.5 kW
Switching Frequency	25 kHz
Low-side Switches	$M_1 \sim M_4$: IRFB4321Pbf
High-side Switches	$M_5 \sim M_8$: IRFP26N60LPbf
Turns Ratio	$N_P / N_S = 1 / 4.26$
Leakage Inductance	$L_{ll} = 0.5$ µH, $L_{lh} = 9$ µH
Current-fed Inductor	$L_m = 500$ µH
High-side capacitor	470 µF * 2
Core of Isolation Transformer	EE-55
Core of Flyback Transformer	EI-40
Snubber Capacitor	C_C : 100 nF
Buffer Capacitor	C_{b1} & C_{b2} : 4.7 nF
Turns Ratio (Flyback)	$N_1 / N_2 / N_3 = 1 / 3 / 3$
Leakage Inductance (Flyback)	1.3 µH

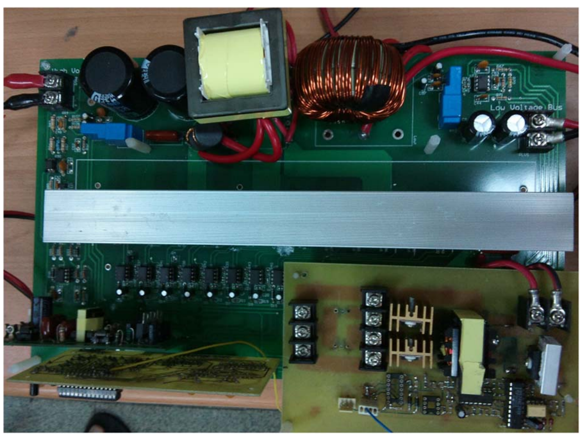

Fig. 9. Photograph of proposed converter (type C).

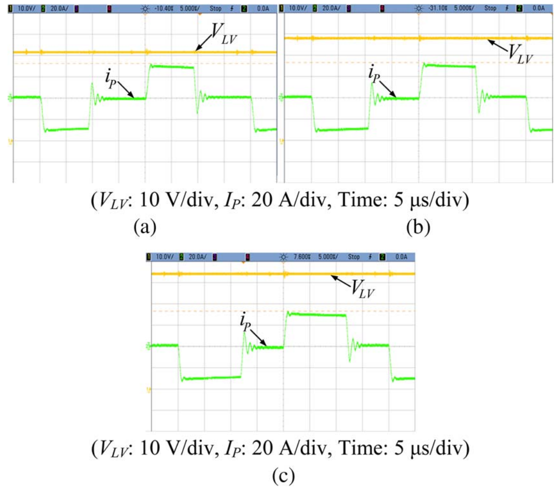

Fig. 10. Measured waveforms of voltage $V_{\rm LV}$ and current i_P from input voltages (a) 42, (b) 48, and (c) 54 V under step-up conversion.

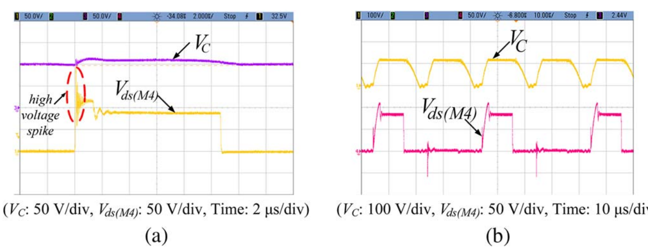

Fig. 11. Measured voltage waveforms of V_C and $V_{ds(M4)}$ from (a) type A, and (b) the proposed one of which V_C is discharged completely in each switching cycle, under step-up conversion and with 1.5-kW power rating.

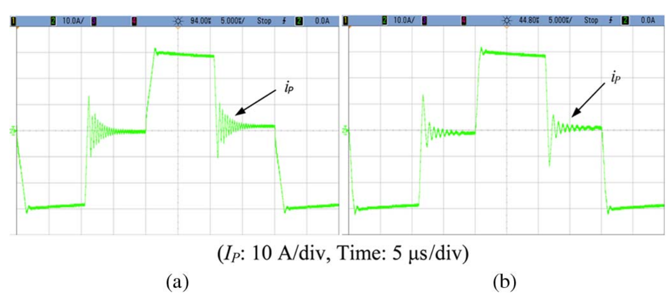

Fig. 12. Measured current i_P waveforms from (a) type A and (b) the proposed one under step-up conversion and with 1.5-kW power rating.

high-side voltage is 360 V. Type C was implemented with the specifications listed in Table I, and a photograph of the 1.5-kW experimental prototype of the proposed converter (type C) is shown in Fig. 9.

In the following discussion, type A will be first compared with the proposed converter to verify that a turnoff soft-switching feature can be achieved in both step-up and step-down conversions. The voltage and current waveforms measured from type B and the proposed one prove that two snubber diodes D_{b1} and D_{b2} are needed to block the ringing current. Then, the current waveforms i_P measured from the converter with an active clamp circuit [13] and the proposed one show that the energy stored in C_C is recycled by the proposed snubbers and its discharging current does not flow through the main switches.

Measured waveforms of low-side voltage $V_{\rm LV}$ and current i_P under step-up conversion are shown in Fig. 10. For the voltage variation of batteries, the proposed bidirectional converter can cover input voltage range from 42 to 54 V.

Measured voltage waveforms of snubber capacitor V_C and $V_{ds(M4)}$ from type A and the proposed one under step-up conversion are shown in Fig. 11. It can be observed from Fig. 11(a) that V_C is regulated to a desired value just slightly higher than $V_{ds(M4)}$ in type A. Since the regulated voltage V_C is slightly higher than $V_{ds(M4)}$, the energy transferred by the flyback snubber is just a small amount. However, the parasitic capacitance of the switches and the stray inductance of the circuit will result in high-voltage spike. In the proposed converter, capacitor C_C is fully discharged, which could result in higher energy transferred by the flyback snubber than type A. Thus, capacitor C_C should be chosen with a smaller capacitance. For type A, the value of C_C is 1 μF, while that of the proposed one is 0.1 μF. Referring to (2), the processed power $P_{\rm FB}$ by the flyback snubber of the proposed one is 36 W, just around 2.4% of the maximum power level. Moreover, the proposed operating scheme can achieve near soft-switching feature for switches $M_1 \sim M_4$ at turnoff transition, and the overshoot voltage can be suppressed to a lower level, as shown in Fig. 11(b). Fig. 12 shows the measured waveform of current i_P from type A and the proposed one. Although capacitor C_C is fully discharged, the proposed passive snubber can hold voltage V_{b1} or V_{b2}.

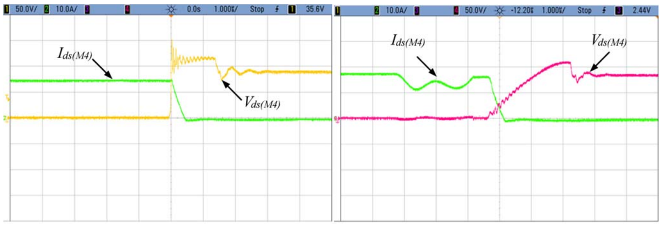

($V_{ds(M4)}$: 50 V/div, $I_{ds(M4)}$: 10 A/div, Time: 1 μs/div)
(a) (b)

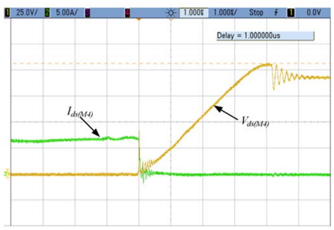

($V_{ds(M4)}$: 25 V/div, $I_{ds(M4)}$: 5 A/div, Time: 1 μs/div)
(c)

Fig. 13. Measured voltage $V_{ds(M4)}$ and current $I_{ds(M4)}$ waveforms at M_4 turnoff transition from (a) type A and (b) the proposed one with 1.5 kW and (c) the proposed one with 500 W, under step-up conversion.

Referring to the following equations, di_P/dt of the proposed one is higher than that of type A, which can reduce duty loss

$$\begin{aligned}\frac{di_p}{dt} &= \frac{V_{AB} - V_{CD} \times \frac{N_P}{N_S}}{L_{\rm eq}} \\ &= \frac{V_{Cc} - (V_{\rm HV} \times \frac{N_P}{N_S})}{L_{\rm eq}} \text{ (Type A)}\end{aligned} \quad (6)$$

$$\begin{aligned}\frac{di_p}{dt} &= \frac{V_{AB} - V_{CD} \times \frac{N_P}{N_S}}{L_{\rm eq}} \\ &= \frac{V_{Cc} - (V_{\rm HV} - V_{Cb1}) \times \frac{N_P}{N_S}}{L_{\rm eq}} \text{ (proposed).}\end{aligned} \quad (7)$$

Fig. 13 shows the measured waveforms of voltage $V_{ds(M4)}$ and current $I_{ds(M4)}$ from type A and the proposed one at M_4 turnoff transition, in which Fig. 13(a) and (b) are with a load of 1.5 kW and Fig. 13(c) is with 500 W. It can be observed that the voltage spike in type A is up to 197 V, due to the parasitic capacitance of switches $M_1 \sim M_4$ and stray inductance on the circuit. On the other hand, the proposed one can not only achieve near ZCS turnoff soft-switching feature but also can alleviate the voltage spike to 107 V, as shown in Fig. 13(b). Moreover, Fig. 13(b) and (c) shows that the soft-switching feature can be achieved at both light- and heavy-load conditions. Fig. 14 shows the measured waveforms of voltage $V_{ds(M8)}$ and current $I_{ds(M8)}$ from type A and the proposed one at M_8 turnoff transition. It can be observed that, with C_{b1} and C_{b2}, $V_{ds(M8)}$ of the proposed converter rises up with a lower slope and the switching loss of $(V_{ds(M8)} \cdot I_{ds(M8)})$ becomes lower, achieving near ZCS turnoff soft-switching feature.

Fig. 15 shows the measured waveforms of voltages $V_{ds(M5)}$ and $V_{ds(M6)}$ from type B and the proposed one under step-down conversion. It can be observed that, due to large buffer capacitors C_{b1} and C_{b2}, voltage V_{ds} of type B is ringing at switching transition, as shown in Fig. 15(a). Fig. 16 shows the measured waveforms of voltages $V_{ds(M5)}$ and V_{b1} and current $I_{ds(M5)}$ from type B and the proposed one under step-down

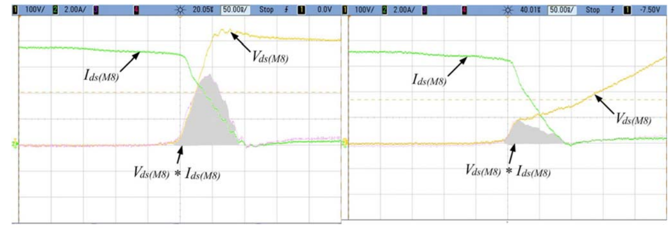

($V_{ds(M8)}$: 100 V/div, $I_{ds(M8)}$: 2 A/div, Time: 50 ns/div)
(a) (b)

Fig. 14. Measured voltage $V_{ds(M8)}$ and current $I_{ds(M8)}$ waveforms at M_8 turnoff transition from (a) type A and (b) the proposed one under step-down conversion and with 1.5-kW power rating.

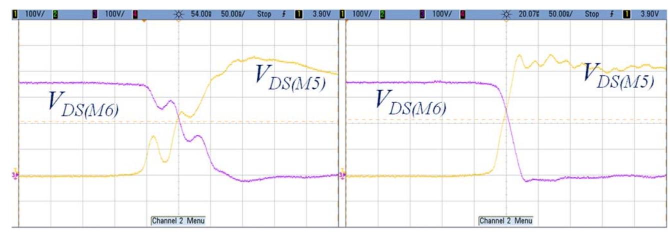

($V_{ds(M5)}$: 100 V/div, $V_{ds(M6)}$: 100 V/div, Time: 50 ns/div)
(a) (b)

Fig. 15. Measured voltage $V_{ds(M5)}$ and voltage $V_{ds(M6)}$ waveforms from (a) type B and (b) the proposed one under step-up conversion and with 1.5-kW power rating.

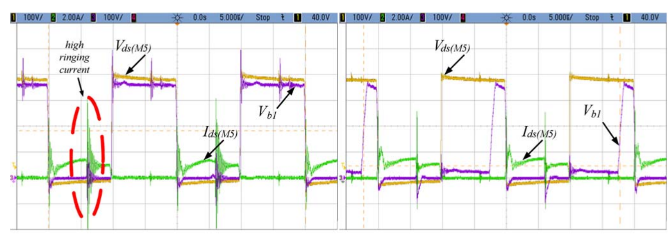

($V_{ds(M5)}$: 100 V/div, $I_{ds(M5)}$: 2 A/div, V_{b1}: 100 V/div, Time: 5 μs/div)
(a) (b)

Fig. 16. Measured voltages $V_{ds(M5)}$ and V_{b1} and current $I_{ds(M5)}$ waveforms from (a) type B and (b) the proposed one under step-down conversion and with 1.5-kW power rating.

conversion. It can be observed from Fig. 16(a) that, because of large buffer capacitors C_{b1} and C_{b2}, there exists high ringing current in type B at switching transition, which will result in high EMI noise and switching loss. On the other hand, the ringing current is much lower in the proposed converter, as shown in Fig. 16(b).

Fig. 17 shows the measured waveform of current i_P under step-up conversion from the converter with an active clamp circuit [13] and the proposed one. It can be observed from Fig. 17(a) that the peak current of i_P under the full-load condition is 48.1 A, which means the discharging current $(48.1 - 30 = 18.1\ \text{A})$ of C_C flowing through the main switches and increasing stress significantly. On the contrary, the energy stored in C_C is recycled by the proposed passive and active snubbers, which can reduce the current stress.

Fig. 18 shows the plots of conversion efficiency versus power level of type A and the proposed one operated in the step-up conversion. The processed power $P_{\rm FB}$ by the flyback snubber in the proposed converter is 36 W, while $P_{\rm FB}$ is 52.5 W in type A. The conversion efficiency of the proposed converter under the full-load condition is about 91.5%. However, since capacitor

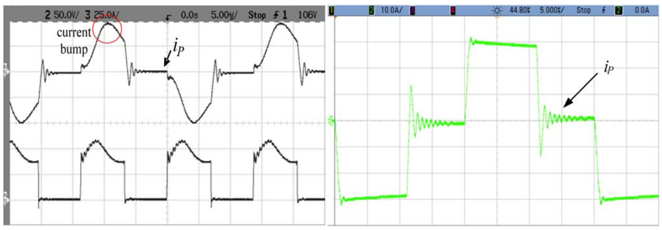

(i_P: 25 A/div, Time: 5 µs/div) (a) (i_P: 10 A/div, Time: 5 µs/div) (b)

Fig. 17. Measured current i_P waveforms from (a) the converter with an active clamp circuit [13] and (b) the proposed one under step-up conversion and with 1.5-kW power rating.

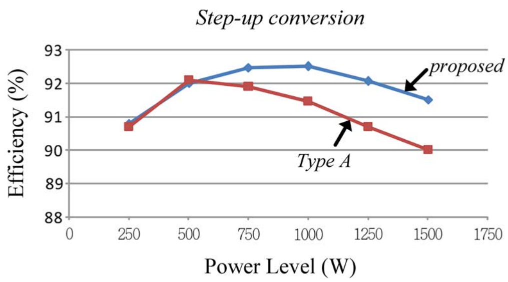

Fig. 18. Plots of conversion efficiency of type A and the proposed one operated in the step-up conversion.

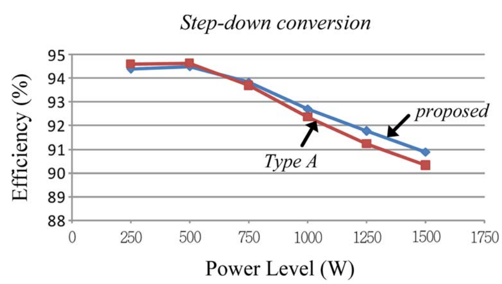

Fig. 19. Plots of conversion efficiency of type A and the proposed one operated in the step-down conversion.

TABLE II
KEY COMPONENT LOSS ESTIMATION UNDER 1.5-kW POWER RATING

Key Components	Loss Estimation	
	Step-up Conversion	Step-down Conversion
Low-side Switches $M_1 \sim M_4$	21.6 W	22.2 W
High-side Switches $M_5 \sim M_8$	4.0 W	6.4 W
Current-fed Inductor L_m	51.9 W	63.8 W
Isolation Transformer T_P	26.8 W	26.8 W
Flyback Snubber	10.8 W	3.3 W
Snubber Diodes D_{b1} & D_{b2}	0.2 W	0.1 W
Total	115.3 W	122.6 W

C_C is fully discharged by the proposed operation scheme, power loss of the flyback snubber results in low efficiency under light-load condition, and the flyback snubber is controlled like that in type A when the load is lower than 500 W. Note that, under light-load condition, there is no voltage spike since capacitor C_C can absorb the current difference between the leakage inductance and the inductor currents. Fig. 19 shows the plots of conversion efficiency versus power level of type A and the proposed one operated in the step-down conversion. It can be observed that the conversion efficiency of the proposed converter is close to that of type A since both of them are operated in similar manner. The key component loss estimation is summarized in Table II.

V. CONCLUSION

This paper has presented a soft-switching bidirectional isolated full-bridge converter, which allows input voltage variation from 42 to 54 V, for battery charging/discharging applications. The proposed converter can reduce the voltage spike caused by the current difference between leakage inductance and current-fed inductor currents, the current spike due to diode reverse recovery, and the current and voltage stresses, while it can achieve near ZVS and ZCS soft-switching features. The passive snubber can hold voltage V_{b1} or V_{b2} and improve the slew rate of di_P/dt, which can reduce duty loss. However, near ZVS turn-on transition cannot be achieved under light-load condition in step-down conversion. Experimental results measured from the three types of 1.5-kW isolated bidirectional full-bridge dc–dc converters have verified that the proposed converter (type C) can yield the performance of lower voltage and current spikes, higher efficiency, and less ringing. It is suitable for high-power applications with galvanic isolation.

REFERENCES

[1] Z. Zhang, O. C. Thomsen, and M. A. E. Andersen, “Optimal design of a push–pull–forward half-bridge (PPFHB) bidirectional DC–DC converter with variable input voltage,” *IEEE Trans. Ind. Electron.*, vol. 59, no. 7, pp. 2761–2771, Feb. 2012.

[2] D. V. Ghodke, K. Chatterjee, and B. G. Fernandes, “Modified soft-switched three-phase three-level DC–DC converter for high-power applications having extended duty cycle range,” *IEEE Trans. Ind. Electron.*, vol. 59, no. 9, pp. 3362–3372, Sep. 2012.

[3] F. Zhang, L. Xiao, and Y. Yan, “Bi-directional forward-flyback DC–DC converter,” in *Proc. IEEE Power Electron. Spec. Conf.*, 2004, vol. 5, pp. 4058–4061.

[4] H. Li, D. Liu, F. Z. Peng, and G.-J. Su, “Small signal analysis of a dual half bridge isolated ZVS bi-directional DC–DC converter for electrical vehicle applications,” in *Proc. IEEE Power Electron. Spec. Conf.*, 2005, pp. 2777–2782.

[5] L.-S. Yang and T.-J. Liang, “Analysis and implementation of a novel bidirectional DC–DC converter,” *IEEE Trans. Ind. Electron.*, vol. 59, no. 1, pp. 422–434, Jan. 2012.

[6] D. Liu and H. Li, “Design and implementation of a DSP based digital controller for a dual half bridge isolated bi-directional DC–DC converter,” in *Proc. IEEE Appl. Power Electron. Conf.*, 2006, pp. 695–699.

[7] B. Zhao, Q. Yu, Z. Leng, and X. Chen, “Switched Z-source isolated bidirectional DC–DC converter and its phase-shifting shoot-through bivariate coordinated control strategy,” *IEEE Trans. Ind. Electron.*, vol. 59, no. 12, pp. 4657–4670, Dec. 2012.

[8] U. K. Madawala, M. Neath, and D. J. Thrimawithana, “A power-frequency controller for bidirectional inductive power transfer systems,” *IEEE Trans. Ind. Electron.*, vol. 60, no. 1, pp. 310–317, Jan. 2013.

[9] D. Aggeler, J. Biela, S. Inoue, H. Akagi, and J. W. Kolar, “Bi-directional isolated DC–DC converter for next-generation power distribution-comparison of converters using Si and SiC devices,” in *Proc. Power Convers. Conf.*, 2007, pp. 510–517.

[10] H. Krishnaswami and N. Mohan, “A current-fed three-port bi-directional DC–DC converter,” in *Proc. Telecommun. Energy Conf.*, 2007, pp. 523–526.

[11] O. Garcia, L. A. Flores, J. A. Oliver, J. A Cobos, and J. de la Peña, “Bi-directional DC–DC converter for hybrid vehicles,” in *Proc. IEEE Power Electron. Spec. Conf.*, 2005, pp. 1881–1886.

[12] S. Yujin and P. N. Enjeti, “A new soft switching technique for bi-directional power flow, full-bridge DC–DC converter,” in *Conf. Rec. IEEE IAS Annu. Meeting*, 2002, vol. 4, pp. 2314–2319.

[13] K. Wang, C. Y. Lin, L. Zhu, D. Qu, F. C. Lee, and J. S. Lai, “Bi-directional DC–DC converters for fuel cell systems,” in *Proc. IEEE Power Electron. Transp.*, 1998, pp. 47–51.

[14] L. Zhu, “A novel soft-commutating isolated boost full-bridge ZVS-PWM DC–DC converter for bidirectional high power applications,” *IEEE Trans. Power Electron.*, vol. 21, no. 2, pp. 422–429, Mar. 2006.

[15] D. J. Thrimawithana, U. K. Madawala, and M. Neath, “A synchronization technique for bidirectional IPT systems,” *IEEE Trans. Ind. Electron.*, vol. 60, no. 1, pp. 301–309, Jan. 2013.

[16] W. Chen, P. Rong, and Z. Lu, "Snubberless bidirectional DC–DC converter with new CLLC resonant tank featuring minimized switching loss," *IEEE Trans. Ind. Electron.*, vol. 57, no. 9, pp. 3075–3086, Sep. 2010.
[17] G. Ma, W. Qu, G. Yu, Y. Liu, N. Liang, and W. Li, "A zero-voltage-switching bidirectional DC–DC converter with state analysis and soft-switching-oriented design consideration," *IEEE Trans. Ind. Electron.*, vol. 56, no. 6, pp. 2174–2184, Jun. 2009.
[18] T.-F. Wu, Y.-C. Chen, J.-G. Yang, and C.-L. Kuo, "Isolated bidirectional full-bridge DC–DC converter with a flyback snubber," *IEEE Trans. Power Electron.*, vol. 25, no. 7, pp. 1915–1922, Jul. 2010.
[19] A. Mousavi, P. Das, and G. Moschopoulos, "A comparative study of a new ZCS DC–DC full-bridge boost converter with a ZVS active-clamp converter," *IEEE Trans. Power Electron.*, vol. 27, no. 3, pp. 1347–1358, Mar. 2011.

Tsai-Fu Wu (S'88–M'91–SM'98) received the B.S. degree in electronic engineering from National Chiao Tung University, Hsinchu, Taiwan, in 1983, the M.S. degree in electrical and computer engineering from Ohio University, Athens, OH, USA, in 1988, and the Ph.D. degree in electrical engineering and computer science from the University of Illinois, Chicago, IL, USA, in 1992.

From 1985 to 1986, he was a System Engineer with SAMPO, Inc., Kuei-Shan Hsiang, Taiwan, where he was involved in developing and designing graphic terminals. From 1988 to 1992, he was a Teaching and Research Assistant with the Department of Electrical Engineering and Computer Science, University of Illinois, Chicago, IL, USA. From 1993 to 2012, he was with the Department of Electrical Engineering, National Chung Cheng University, Minxiong, Taiwan. He is currently a Professor with the Department of Electrical Engineering, National Tsing Hua University, Hsinchu. His current research interests include developing and modeling of power converters; design of electronic dimming ballasts for fluorescent lamps, metal halide lamps and plasma display panels; design of solar-array supplied inverters for grid connection; and design of pulsed-electrical-field generators for transdermal drug delivery and food pasteurization.

Dr. Wu is a Senior Member of the Chinese Institute of Engineers. He was the recipient of three Best Paper Awards from the Taipei Power Electronics Association in 2003–2005. In 2006, he was named as an Outstanding Researcher by the National Science Council, Taiwan.

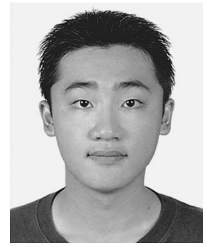

Jeng-Gung Yang was born in Taiwan in 1985. He received the B.S. and M.S. degrees in electrical engineering from National Chung Cheng University, Minxiong, Taiwan, in 2009 and 2011, respectively, where he is currently working toward the Ph.D. degree in the Department of Electrical Engineering.

His current research interests include the design and development of soft-switching power converters.

Chia-Ling Kuo was born in Taiwan in 1985. She received the B.S. and M.S. degrees in electrical engineering from National Chung Cheng University, Minxiong, Taiwan, in 2008 and 2010, respectively, where she is currently working toward the Ph.D. degree in the Department of Electrical Engineering.

Her research interests include the design and implementation of bidirectional inverters for dc-distribution applications.

Yung-Chun Wu was born in Kaohsiung, Taiwan, in 1971. He received the Ph.D. degree in electrical engineering from National Chung Cheng University, Minxiong, Taiwan, in 2000.

From 2000 to 2001, he was an Assistant Professor with the Department of Electrical Engineering, Chienkuo Institute of Technology, Changhua, Taiwan. From 2001 to 2007, he was an Assistant Professor with the Department of Electrical Engineering, I-Shou University, Kaohsiung, Taiwan. Since 2007, he has been with the Department of Aeronautical Engineering, National Formosa University, Huwei, Taiwan, where he is currently an Assistant Professor. His research interests include developing and designing converter topologies, electronic ballasts, and high-efficiency converters.